Thermodynamics of Black Powder and Aerodynamics of Propelled Aerial Shells

John E. Mercer
18906 107th St. Ct. KPN, Gig Harbor, WA, 98329, USA

ABSTRACT

This paper describes the theoretical basis of a computer code that numerically models firework mortars. The code analyzes both the Black Powder propelling and flight segments of a shell. Equations for the gas dynamics of Black Powder combustion, leakage flow around the shell and aerodynamics of flight are included. Representations for commonly used Black Powder grain sizes allow for simple modeling of test cases. The numerical equation solver in the code uses standard parameters for specifying any mortar test condition. This solver computes every model parameter of the gas and shell dynamics in 2 μs time steps while in the mortar and in 1 ms time steps in flight. The modeling demonstrates that the release of energy from Black Powder is a multi-step process, first from the burning of the grains, next from the latent heat release from condensation, and finally from the latent heat release from fusion. The shell flight dynamics are based on aerodynamic theory employing conventional parameters. Uses of this code include design of mortars, and parametric and safety analyses. The code even includes a crosswind drift analysis for predicting expected dud fallout location. The analytic models were verified on a multitude of test cases, taken from both firework mortars and muzzle loading firearms data. Agreement with the experimental data is within the experimental measurement variation.

Keywords: mortar, latent heat, Black Powder, thermodynamics, aerodynamics, leakage flow, shell drift, muzzle velocity, drag

Introduction

Most people have a fascination with fireworks. In 2001 after viewing a 4th of July display, the author wondered if the dynamics of the mortar firing and shell flight could be modeled to provide an accurate prediction of flight performance. Accurate height predictions and velocity profiles could be used to improve display design, while accurate predictions of mortar pressures and dud fallout location could make fireworks performances safer.

In an effort to address these issues, the author conceived a simple model based on adiabatic, isentropic expansion. The model was programmed in a short time, but the results did not match the available data. This quick, analytical model evolved into more than a 6-month effort that was a major technical challenge.

The initial, simple model assumed that the burning produced packets of compressed gas that would expand isentropically, producing a pressure that would propel the shell from the mortar. Efforts to find any papers or texts on the burning of Black Powder produced references by Conkling,[1] Davis,[2] Shimizu,[3–5] Shidlovskiy,[6] von Maltitz,[7] Sassé,[8] Jones[9] and Freedman.[10] Davis presents extensive information on the products of combustion of Black Powder, including the heat of explosion and combustion temperature. Shidlovskiy presents a model for the burning rate, specific heats as a function of temperature, and approximations for the heats of vaporization and fusion. A burning model and a representative model for the Black Powder grains were developed based on these references. From these models a code was produced for generating the packets of compressed gas. The effort then turned to finding experimental data that could verify the modeling. This search led to articles in the *Journal of Pyrotechnics*[11] and to Shimizu's[12] *Fireworks from*

a Physical Standpoint. Recently the work of Contestabile[13,14] was brought to the authors' attention. Although the extensive experimental parametric study by Contestabile was not included in the comparisons presented here, it should be key to further refinements of the model.

Shimizu' work[12] contains both experimental data and a parametric model for the mortar firing dynamics. Using the parametric model, Kosanke[11] performed a study of the sensitivity of mortar dynamics to parameter variations. Shimizu's model was based on equations developed for smokeless powder. However, smokeless powder produces entirely gaseous products while Black Powder has substantial nongaseous products. As will be shown, these nongaseous products play a major role in the gas expansion process. The Shimizu model, therefore, can only account for small perturbations from the basic model. Regardless of the model, the experimental data were excellent.

In an effort to verify any proposed universal model, data from the other end of the spectrum from firework mortars was sought. This search led to Black Powder muzzle loading data sources.[15] These data extremes were used to validate the isentropic model. The test validations revealed that the isentropic expansion model was not accurate and did not follow the data trends. Several patches and "fudge factors" were added to the model, but they did not produce the correlation expected of a good model. The simple model was abandoned.

The revised analysis was based on the fundamentals of thermodynamics. The fundamental model revealed, as mentioned above, that the particulate matter, which had been ignored in the earlier analysis, was critical to the modeling. In fact it was discovered that the delayed release of heat from the phase transitions of condensing and solidifying products of combustion were key elements to the propelling characteristics of Black Powder.

This paper describes the analytical model that accurately predicts the burning and gas dynamics of Black Powder as a propellant including leakage effects during shell launch. It also describes the aerodynamic model that predicts the flight characteristics of shells including drift due to crosswinds. A description of the numerical code that solves the equations for these models presents the input and output parameters currently used.

Models Used in the Program

Black Powder Thermodynamics

The first law of thermodynamics provides the fundamental concept for modeling the forces acting on the shell to accelerate it while in the mortar. The first law is expressed in differential form as:

$$\frac{dU}{dt} = \frac{dQ}{dt} - \frac{d\int PdV}{dt}$$

where U is the internal energy, Q is the heat, P is the gas pressure and dV is the change in volume of gases. The integral

$$\int PdV$$

represents the work done.

The internal energy, U, is generally expressed as:

$$U = C_v T$$

where C_v is the specific heat at constant volume and T is the temperature of the gas. The left side of the first law equation becomes:

$$\frac{dU}{dt} = C_v \frac{dT}{dt} + T\frac{dC_v}{dt}$$

The second term reflects the change in specific heat, C_v, with temperature. Specific heat for a gas depends on whether the gas molecule is monatomic, diatomic or polyatomic. The variation is due to the different degrees of freedom of motion for the different molecular structures. The value of C_v is relatively constant at near ambient temperatures, but at higher temperatures the value increases because of additional degrees of freedom associated with intramolecular vibrational modes.

The heat term, Q, has two components. The first component is the immediate heat released at the instant of combustion, and a second component is associated with the delayed release of heat due to phase changes of the combustion products.

Table 1. Black Powder Data Based on Davis.[2]

Heat of explosion = 718.1 cal/g
Explosion temperature = 2770 °C

Mass of gases/mass of Black Powder = 0.4298
Mass of solids/mass of Black Powder = 0.5591
Mass of water/mass of Black Powder = 0.0111
Moles of gas/kilogram of Black Powder= 12.14
Average gram molecular mass of gases = 35.41

Gases		Solids			Temperature (°C)		Vapor Phase		
Volume (%)		Mass (%)		Mol Mass	Fusion	Vapor.	Particles	(%)	Mol Mass
CO_2	49.29	K_2CO_3	61.03	138.21	891	d	K_2O	41.59	94.19
CO	12.47	K_2SO_4	15.10	174.27	588	1689	CO_2	19.44	44.01
N_2	32.91	K_2S	14.45	110.27	840		K_2SO_4	15.10	174.27
H_2S	2.65	KNCS	0.22	97.18	173.2	d 500	K_2S	14.45	110.27
CH_4	0.43	KNO_3	0.27	101.11	334	d 400	KNCS	0.22	97.18
H_2	2.19	$(NH_4)_2CO_3 \cdot H_2O$	0.08	114.1	d 58		KNO_3	0.27	101.11
54.56%		S_8	8.74	256.5	112.8	444.7	$(NH_4)_2CO_3 \cdot H_2O$	0.08	114.1
polyatomic		C	0.08	12.01	4827	4827	S_8	8.74	256.5
45.38%							C	0.08	12.01
diatomic		Average gram molecular mass of solids = 149.6 Average atoms/molecule = 5.27			Average Fusion Temperature = 1042 K		Average gram molecular mass of vapor = 113.0		

Notes: K_2O will also dissociate according to Reference 16. This effect was found to have a negligible impact on the results.
Mass and temperature data provided by Reference 16.

Table 1, taken mainly from data provided by Davis,[2] provides the characteristics of Black Powder used in the model. The heat of explosion, Q_{exp}, and the weights and volumes of the products of combustion were used directly with one modification. Potassium carbonate, K_2CO_3, the main component of the condensed products, does not exist as a vapor. The model treats K_2CO_3 the same as the other nongaseous components, below the vaporization temperature, to calculate the mean fusion temperature but assumes that it dissociates above the fusion temperature.

Rather than having individual vaporization and fusion temperatures associated with each of the phase changing products* of combustion, the model was simplified by having only one representative vaporization and one representative fusion temperature. A mean value is used for the fusion temperature based on published data.[16] No comprehensive data could be found for the vaporization and dissociation temperatures so a single vaporization-dissociation temperature was determined by adjusting the temperature to give the best comparison of the model's predictions to the available experimental data.

Shidlovskiy[6] provides average values for C_v over a temperature range for the different molecular structures (i.e., monatomic, diatomic and polyatomic). These values were used to compute a segmented-linearized approximation to the temperature variation of specific heat for each of the molecular structures. Scaling, corresponding to the instantaneous mix of constituents, is used to calculate instantaneous values of C_v. The constituents of air are diatomic (excluding the trace components) so the diatomic C_v value is used for it. Derivatives of C_v are calculated from the linearized approximation.

Numerical experimentation, using the complete code to minimize the error between computed and experimental results, provided the following temperatures and heat parameters for Black Powder:

* The term "phase changing products" refers to those products of combustion that eventually become solid but are formed initially as gases.

$$T_{vap} = 2400 \text{ K}$$
$$T_{fus} = 1042 \text{ K}$$
$$Q_{vap} = 4.44 \times 10^6 \text{ J/kg}$$
$$Q_{fus} = 6.85 \times 10^5 \text{ J/kg}$$

where T_{vap} is the vaporization temperature, T_{fus} is the fusion temperature, Q_{vap} is the latent heat of vaporization, and Q_{fus} is the latent heat of fusion.

These heat values, determined by the model, indicate that only 5% of the total heat is released at the instant of combustion while the other 95% is released subsequently. These model heat values indicate that 82% of the heat of explosion is associated with the latent heat of vaporization and ionization energy while 13% of the heat of explosion is associated with the latent heat of fusion. The author believes that much of the heat of combustion goes into ionizing the products of combustion. Davis[2] provides an experimental measurement for the combustion temperature of Black Powder as 3043 K. This temperature is well above the temperatures for fusion and vaporization and most likely produces most or all of the combustion products in an ionized state. The current model does not include ionizing energy effects, and as a consequence, the numerical experimentation results presented above produced values that did not comply with the approximate formulas specified by Shidlovskiy.[6] The heat of vaporization was 60% of the formula value while the heat of fusion value was twice the formula value, yet the overall match to the experimental data is good. By not specifically providing a model for the ionic energy release mechanism, the model accommodates this phenomenon by altering the available modeling parameters, including the apparent vaporization temperature, drawing it closer to the combustion temperature and reducing the apparent heat of vaporization as compared to Shidlovskiy's approximation. The computed heat of fusion is also affected, producing a greater heat release at the mean fusion temperature. The numerical error minimization procedure produced these values so that the heat release model would closely approximate the actual physical heat release. The next generation model should include a separate model for the latent ionic energy release to provide a better overall heat release model.

The modeling revealed that approximately 3 to 15% of the available latent heat of vaporization/ionization is released as the projectile moves through the barrel or mortar. The model also revealed that there was negligible heat released from the fusion process since the muzzle temperatures of the test cases were at or above the fusion temperature. For the particular cases modeled, the time from combustion initiation to projectile exit ranged from 1.1 to 13 ms. This means that the time scale for latent heat release is of the order of milliseconds. As will be shown later in this paper, the rate of heat release depends on both time and the gas expansion profile that determines the instantaneous gas temperature. The latent heat release is therefore a critical factor in the thermodynamics of the process since the energy released from latent heat is of the same order of magnitude as the energy released at the instant of combustion.

Black Powder Particle Model

Table 2 provides the screen sizes for various industry standard grain sizes.[11,12,17] Shimizu,[4] Sassé,[8] and Jones[9] considered various modeling of the Black Powder grains. Some of the authors used ellipsoidal shapes while others used a combination of spheres and cubes. Although the particles have irregular shapes, the author decided to represent the particles as spheres with an equal radius probability distribution over the range from minimum to maximum screen size. Since the burning rate is related to the surface area, a weighted average based on surface area is used to model the particle. The equations describing the model are:

$$\frac{dN}{dr} = K$$
$$N = \int_{r_{min}}^{r_{max}} K \, dr = K\left(r_{max} - r_{min}\right)$$
$$r_{mean}^2 = \frac{1}{N}\int_{N_{min}}^{N_{max}} r^2 dN = \frac{1}{N}\int_{r_{min}}^{r_{max}} r^2 K \, dr$$
$$r_{rms} = \sqrt{\frac{\left(r_{max}^3 - r_{min}^3\right)}{3\left(r_{max} - r_{min}\right)}}$$

where N is the number of particles and K is the probability distribution constant. The mean radius, r_{rms}, represents the particle with the root mean square area. The number of particles of Black Powder in the powder charge is:

Table 2. Black Powder Screen Sizes.

Designation	Radius Values (cm)		Ref.
	Min. Size	Max. Size	
FA	0.20	0.40	12
2FA	0.084	0.24	12
3FA	0.060	0.10	12
4FA	0.042	0.084	12
5FA	0.015	0.042	12
6FA	0.015	0.030	12
7FA	0.0075	0.021	12
Meal D	0.0	0.021	12
Fg	0.060	0.084	12
2Fg	0.030	0.060	12
3Fg	0.015	0.042	12
4Fg	0.0075	0.021	12
0	0.020	0.060	6
1	0.010	0.020	6
2	0.020	0.060	6
3	0.060	0.085	6
4	0.12	0.17	6

$$N_{BP} = \frac{M_{BP}}{\frac{4}{3}\pi r_{rms}^3 \rho_{BP}}$$

where ρ_{BP} is the density of Black Powder particles, assumed to be 1750 kg/m^3.

There are some differences between the shapes of powders of different granulation. For example, the Fg powders are glazed while the FA powders are not. Glazing tends to eliminate sharp edges and to make the grains closer to spherical. These differences can be handled in the model by adjusting the apparent particle burn rate based on the changing geometry as the particle burns. The author did not have sufficient experimental data to resolve this effect, so the spherical model was used for all granulations.

Ignition Propagation Rate Model

The propagation of flame through the particles is modeled as an exponential function. The underlying assumption is that the rate of increase of ignition is proportional to the number of ignited particles.

$$N = N_0 e^{P_r t}$$

where N_0 is the initial number of particles ignited by the fuse or percussion cap and P_r is the propagation rate. Numerical experimentation yielded a propagation rate of 5000 particles per second for a good match to the available data. The value of N_0 for fuse ignition is set to 0.1 N_{BP} while that for percussion cap ignition is set to 0.5 N_{BP}. Numerical experimentation did not show a strong dependence on this initial value since the propagation rate is very fast compared to the total burn time.

Burn Rate Model

The burn rate model is taken from a combination of models presented in Shidlovskiy[6] and Conkling.[1] The burn rate is given by,

$$\frac{dr_{BP}}{dt} = Be^{\alpha T_{BP}} P_{atm}^{\eta}$$

where r_{BP} is the radius of the Black Powder particle, T_{BP} is the temperature of the Black Powder in °C, P_{atm} is the pressure of the gases in atmospheres, α is the exponential temperature dependence coefficient, B is the linear burn rate at standard conditions and η is the exponential dependence of burn rate on pressure. An optimized fit of the models to the experimental data taken from references 12 and 15, showed that the value of B is 0.0115 m/s, slightly less than the value given by Conkling and Shidlovskiy. The optimized value of η was found to be 0.30, slightly greater than that given by Conkling and Shidlovskiy. Since the available experimental data were recorded at near standard temperatures, the value for α was set to 1.5×10^{-3}/°C, the average value specified in Shidlovskiy.

The burning of the Black Powder produces an immediate heat release equal to the change in mass times the heat of explosion less the latent heats of vaporization and fusion.

$$\frac{dQ}{dt} = 4\pi r^2 \rho_{BP} \frac{dr_{BP}}{dt}\left(Q_{exp} - Q_{vap} - Q_{fus}\right)$$

where ρ_{BP} is the density of the Black Powder particle as defined above, Q_{exp} is the heat of explosion per unit mass and Q_{vap} and Q_{fus} are the latent heats per unit mass of the burning products that participate in the phase change model described below. The value of Q_{exp} used in this study is 3.014×10^6 J/kg as specified in Davis.[2]

Latent Heat Release Model

The phase changing components of combustion, which eventually become solid particles, are assumed to be produced as gases that cool by radiation and convection heat transfer at a rate based on the surrounding gas temperature. To simplify the modeling, the delayed release of sensible heat from these components is ignored since it is much less than their latent heats of vaporization and fusion. As the combustion process progresses, a portion of the gases cool and condense into liquids releasing their heat of vaporization. Further cooling releases their heat of fusion.

The cooling of these phase changing components consists of two mechanisms, as stated above: radiation and convection. The rate of mass phase conversion per unit mass due to radiation is dependent on the fourth power of the temperature and is modeled as:

$$R_v = k_R \left(T_{vap}^4 - T^4 \right)$$

where R_v is the rate of mass phase conversion per unit mass kg/kg-s due to condensation of vapor, k_R is the coefficient of the conversion rate, T_{vap} is the vaporization temperature and T is the gas temperature.

For transition through the fusion regime the relation becomes:

$$R_f = k_R \left(T_{fus}^4 - T^4 \right)$$

The variables are defined as above except that the fusion temperature, T_{fus}, replaces T_{vap}. The rate coefficient k_R is assumed to be the same for both phases. Numerical experimentation provided a value of 5.0×10^{-14}/s-$(K)^4$ for k_R.

The rate of mass phase conversion per unit mass due to convection was assumed to be proportional to the temperature difference and the rate of molecular collisions. This rate is a function of the molecular density of the gaseous constituents, ρ_{mole}, and the speed of the molecules, which is proportional to $\sqrt{T}$. The rate of mass phase conversion per unit mass kg/kg-s due to convection is:

$$C_{vap} = k_C \rho_{mole} \sqrt{T} \left(T_{vap} - T \right)$$

where k_C is the proportionality constant found to be 2.5×10^{-6} m^3/s-mol-$(K)^{3/2}$ by an optimization study.

For the fusion regime the formula remains the same except for substitution of T_{fus} for $T_{vap.}$

$$C_{fus} = k_C \rho_{mole} \sqrt{T} \left(T_{fus} - T \right)$$

The rate of conversion of the total mass from one regime to another is the rate of mass conversion per unit mass times the mass undergoing conversion:

$$\frac{dM_{(gas \leftrightarrow liquid,\, liquid \leftrightarrow solid)}}{dt} = \left(R_{(vap,fus)} + C_{(vap,fus)} \right) M_{(gas,liquid,solid)}$$

where $M_{(gas \leftrightarrow liquid)}$ is the mass of condensing vapor or vaporizing liquid (in the vapor transition regime) and $M_{(liquid \leftrightarrow solid)}$ is the mass of solidifying liquid or fusing solid (in the fusion transition regime). The choice of the mass value on the right hand side of the equation depends on the temperature of the gas relative to the phase transition temperature. For example, for a temperature above the fusion temperature, the appropriate mass to use is the solid mass and for a temperature below the fusion temperature the appropriate mass is the liquid mass. The calculation of these masses is described in detail later in this section. The heat release is then:

$$\frac{dQ}{dt} = \frac{dM_{(gas \rightarrow liquid)}}{dt} Q_{vap} + \frac{dM_{(liquid \rightarrow solid)}}{dt} Q_{fus}$$

where Q_{vap} and Q_{fus} are the latent heat values per unit mass (vaporization or fusion).

The mass conversion calculation is part of the latent heat model. The basic scenario for mass conversion modeling is that the burning powder creates gases that will eventually become particles, first liquid then solid particles. This gaseous mass is M_{gas}. The net rate of change of the mass of gas is:

$$\frac{dM_{gas}}{dt} = \kappa \frac{dM_{BP}}{dt} - \frac{dM_{(gas \rightarrow liquid)}}{dt}$$

where dM_{BP}/dt is the mass burn rate of the Black Powder, κ is the fraction of the Black Powder mass that is converted to gaseous components that participate in the latent heat release, and dM_{gas}/dt is the net rate of increase in

the mass of gas. If the temperature of the gases is below the vaporization temperature then $dM_{(gas \rightarrow liquid)}/dt$ will be positive and will remove mass from the gas phase. If it is negative, it will add mass to the gas phase by converting liquid.

The net rate of change of the liquid particle mass is:

$$\frac{dM_{liquid}}{dt} = \frac{dM_{(gas \rightarrow liquid)}}{dt} - \frac{dM_{(liquid \rightarrow solid)}}{dt}$$

where dM_{liquid}/dt is the rate of increase of the liquid mass.

The net rate of change of solid particle mass is:

$$\frac{dM_{solid}}{dt} = \frac{dM_{(liquid \rightarrow solid)}}{dt}$$

If the temperature is above the fusion temperature, any solid mass will be converted to liquid mass and dM_{solid}/dt will be negative.

The mass of matter residing in each phase is tracked using the above equations. This mass in each phase is represented as $M_{(gas,liquid,solid)}$ in the prior equations for computing the latent heat release.

Pressure Model

Freedman[10] and Belov[18] address the non-ideal effect of extreme pressure. Although the pressures in the mortar barrel are high, the author felt that they were not extreme enough to significantly influence the results for fireworks mortars; therefore these non-ideal effects are not included in the present model. The pressure model uses the perfect gas relationship for computing the combustion pressure:

$$P_{comb} = \frac{nR_{const}T}{V}$$

where R_{const} is the universal gas constant, n is the instantaneous total number of moles of gaseous constituents present and V is the volume of the combustion chamber less the volumes of the unburned Black Powder, the condensed matter and the volume of the shell that extends below the reference plane (below the equator for a spherical shell and the bottom of a cylindrical shell). The temperature, T, is calculated from the internal energy term in the first law equation. The volume, V, comes from the dynamic equations for the shell movement.

Leakage Model

The last element of the combustion dynamics model is the calculation of gas and particulate matter leakage around the shell. The model assumes that the gases and condensed particulates are a homogeneous blend and are therefore proportionately ejected through the gap. It ignores any unburnt particles of Black Powder that might be ejected from the combustion volume. The basis for the last assumption is the density and initial size of the Black Powder particles. Inertial and gravitational forces more heavily influence the large particles and tend to keep them in place. When the unburnt particles become smaller and more easily transported by the flowing gases, their persistence becomes very short and therefore less likely to transport significant mass through the gap.

Several different model possibilities were examined. The one chosen that most closely matches the data is based on compressible isentropic flow with the momentum equation altered to accommodate the nongaseous particulate matter. The derivation of the isentropic flow equations can be found in gas dynamics texts such as Shapiro.[19] The compressible flow model limits the Mach number through the narrowest portion of the gap between the shell and the barrel to ≤ 1. Increasing the chamber pressure beyond a critical pressure will cause the flow to "choke" and the Mach number will remain at 1. The critical ratio of the pressure ahead of the shell to the combustion pressure is:

$$r_{crit} = \left(1 + \varepsilon \frac{\overline{\gamma} - 1}{2}\right)^{-\frac{\overline{\gamma}}{\overline{\gamma} - 1}}$$

where $\overline{\gamma}$ is the average ratio of specific heats (C_p/C_v) and ε is the ratio of total mass (gas + particulate) to the mass of the gas alone. C_p is the specific heat at constant pressure and is equivalent to $C_v + R_{const}$. The density of the gas as it passes through the gap between the shell and the barrel is then:

$$\rho_{gap} = \overline{\rho}\, r^{\frac{1}{\overline{\gamma}}} \qquad r \geq r_{crit}$$

where $\overline{\rho}$ is the bulk density of the gas components in the combustion volume and r is the ratio of the pressure ahead of the shell to the combustion pressure. If r is < r_{crit} then r is set to r_{crit} to model the choking effect.

The speed of sound in the gap, a, is given by:

$$a = \sqrt{\frac{\overline{\gamma}\ P_{comb} r}{\rho_{gap}}} \qquad r \geq r_{crit}$$

The Mach number, M, of the gas flow through the gap is given by:

$$M = \sqrt{\frac{r^{-\left(1-\frac{1}{\overline{\gamma}}\right)} - 1}{\varepsilon \frac{\overline{\gamma}-1}{2}}} \qquad r \geq r_{crit}$$

The velocity through the gap, v_{gap}, is then:

$$v_{gap} = aM$$

The leakage fraction rate, dL/dt, is defined as the rate of gas mass loss divided by the total gas mass in the combustion chamber:

$$\frac{dL}{dt} = C_f v_{gap} \left(A_{gun} - A_{shell} \right) \frac{\rho_{gap}}{\overline{\rho}\ V}$$

C_f is a flow coefficient to account for viscous and non-uniform flow effects. Viscosity will reduce the flow velocity on the wall of the barrel and on the surface of the shell, causing a reduction of the overall flow rate. C_f was numerically determined from an optimization study to be 1.0 for round shells, in other words the viscous effects were negligible. For cylindrical shells the viscous effect is expected to be much greater since the length of the gap is much greater. The greater gap length will cause a thicker boundary layer that will reduce the effective gap flow area. There may also be other effects that influence cylindrical shell leakage such as deformations or non-concentric motion in the mortar. The terms in parentheses in the above equation represents the gap area. A_{gun} is the mortar cross-sectional area based on the internal diameter of the mortar and A_{shell} is the shell cross-sectional area based on the outside diameter of the shell. Assuming a homogeneous mix of all the constituents, this leakage fraction term also represents the rate of loss of each of the constituents at any instant. As this factor accounts for the loss of constituents, the burning of the powder adds to the constituents causing the mix to change with time.

Shell Dynamics in Barrel Model

The shell dynamics model assumes that the pressure is uniform on both the combustion chamber side of the shell and the opposite side of the shell. The pressure on the opposite side is calculated by assuming that, as the shell leaves the mortar, the air ahead of it must be pushed out as a slug moving at the speed of the shell. Correspondingly, the pressure acting on the shell is the total pressure:

$$P_{total} = \frac{1}{2} \rho_{air} v_{shell}^2 + P_{air}$$

where P_{air} is the ambient air pressure.

Having defined the equations for the pressure acting on the shell, the complete dynamic equation for the shell movement is:

$$\frac{d^2 x_{shell}}{dt^2} = \frac{\left(P_{comb} - P_{total} \right) A_{shell}}{m_{shell}} - g$$

where x_{shell} is the shell position along the barrel axis, m_{shell} is the mass of the shell and g is the gravitation acceleration constant. This assumes the mortar is fired vertically, if not, then the vector component of the gravitational acceleration along the barrel must be substituted for g. This equation is integrated to calculate the velocity and integrated again to compute the position within the barrel.

Shell Flight Model

Once the shell leaves the barrel more complex aerodynamic forces will act on it. These forces will depend on air density, air viscosity, shape and surface roughness of the shell, etc. The current model has been verified only for spherical shells and the experimental comparisons will only focus on this configuration. The classical source of data on the aerodynamics of spheres is from Hoerner.[20] There have also been studies on the aerodynamics of baseballs.[21] All these studies show similar results for the drag characteristics. The drag on a body moving through the air has a basic dependence that is represented by:

$$D_{shell} = \frac{1}{2}\rho_{air} v^2 C_D(R_N) A_{shell}$$

where C_D (R_N) is the drag coefficient and is a function of the Reynolds number, R_N. $1/2\rho_{air}v^2$ is the dynamic pressure. The Reynolds number is defined as:

$$R_N = \frac{\rho_{air} v d_{shell}}{\mu_{air}}$$

Here, ρ_{air} is the air density, v is the shell velocity, d_{shell} is the diameter of the shell and μ_{air} is the viscosity of air. All the data show that at low speed (low R_N), C_D (R_N) is higher than at high speeds as shown in Figure 1. This is caused by a laminar boundary layer that separates from the shell near the maximum diameter at slow speed (low Reynolds number). At higher speeds the boundary layer becomes turbulent and remains attached past the maximum diameter. The increased extent of attached flow lowers the drag coefficient.

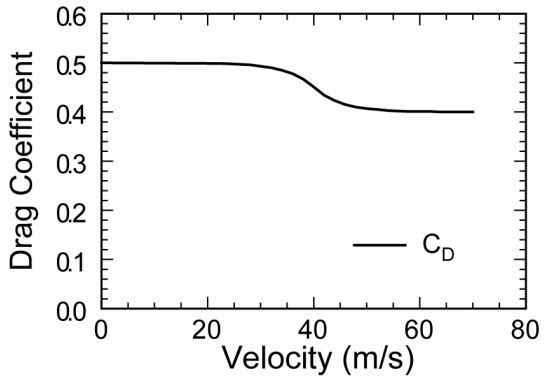

Figure 1. Drag coefficient of a sphere as a function of velocity

A simple model for the drag on a shell is to have one drag coefficient below a transition Reynolds number and another above that transition number. All the experimental data[20,21] show that the transition Reynolds number, R_T, is approximately 400,000. These data also show that the magnitude of the two drag coefficients varies with the surface roughness of the sphere and that the coefficient transitions smoothly from one drag coefficient to the other over a range of Reynolds numbers.

The drag model used in the current study uses two exponential functions to provide this smooth transition:

$$C_D(R_N) = C_{D_{min}} + \left(C_{D_{max}} - C_{D_{min}}\right) e^{\frac{R_T - R_N}{\Delta R_N}} \qquad R_N \geq R_T$$

$$C_D(R_N) = C_{D_{max}} - \left(C_{D_{max}} - C_{D_{min}}\right) e^{\frac{R_N - R_T}{\Delta R_N}} \qquad R_N < R_T$$

ΔR_N was set to 50,000 to match experimental data. Comparisons were made with the experimental data. The results set $C_{D_{min}}$ at 0.4 and $C_{D_{max}}$ at 0.5. These values compare favorably with Shimizu[4] who used a single value of 0.472 in his model without any Reynolds number variation.

The above discussion pertained to spherical shells; however the basic drag model can be used for cylindrical shells as well. Cylindrical aerial shells generally do not have longitudinal stabilization so they tumble through the air. This affects both the reference cross-sectional area and the drag coefficient. A proposed model for cylindrical shells assumes the area for the reference in the drag equation is the average area exposed to the flow:

$$A_{ref} = 0.5\left(\frac{\pi d_{shell}^2}{4} + d_{shell}\ l_{shell}\right)$$

where d_{shell} and l_{shell} are the diameter and length of the cylindrical shell, respectively. The drag coefficient and the dependence on Reynolds number remains to be determined from experimental data but is expected to be between 0.5 and 1.0.

One limitation of this model is that the flow velocity over the shell must not approach the speed of sound where compressible effects would impact the drag. For spheres, the shell velocity that produces sonic flow over the shell is about half the speed of sound. Most fireworks shells should not encounter sonic flow effects, but firearm projectiles would generally operate at and beyond the sonic regime.

One last consideration is the force of gravity on the shell. As the shell exits the barrel, the dominant force is the aerodynamic drag, but as

the shell approaches apogee and the velocity is greatly diminished, gravity becomes the dominant force.

The equation of motion for a shell fired from a vertically oriented mortar, accounting for both aerodynamic drag and gravitational force, is:

$$\frac{d^2 x_{shell}}{dt^2} = -\frac{D_{shell}}{m_{shell}} - g$$

Solving this equation for vertical position, x, and velocity, $\frac{dx}{dt}$, provides the apogee, the impact velocity, if the shell remains intact and returns to $x = 0$, and the elapsed times associated with theses locations.

As discussed above, if the shell is not fired vertically, the forces are divided into the vector components and integrated to compute the velocities and displacements along the additional coordinates.

The numerical code for the flight analysis also incorporates the effects of side winds. The side wind is added vectorially to the shell velocity to produce a new dynamic pressure, and the drag vector is aligned with the total velocity vector. This results in the drag having two components: one aligned with the initial direction of flight and the other transverse to that direction. This produces two differential equations, one for each direction, which must be solved. The side wind model is used to calculate drift for both the apogee position and dud fallout location.

Numerical Equation Solver

All the above equations were incorporated in a numerical solver. The solver is a simple time step routine that updates the variables every 2 µs for the combustion model (shell in mortar) and every 1 ms for the free-air model (shell in flight). The solving process starts with an initial set of conditions computed from the input parameters. The void in the combustion chamber is assumed to be filled with air at ambient conditions (also specified). The dynamic equation solver calculates the amount of Black Powder burned over a time step. This calculation is based on the ignition propagation model and the burn rate model previously discussed. Ignited particles will have a burn rate that depends on how much time has elapsed from the ignition time. Eventually particles will burn away and no longer contribute to the process. The sum of the individual burn rates from all the ignited particles provides the total burn rate for a time step. The numerical process is a discretized convolution integral with the burn rate model being the kernel function. Then, using the burn rate result, the code calculates the new constituent mix and heat added. The heat added from the burned Black Powder and the latent heat released from phase changes cause a change in the internal energy, altering the temperature. The new temperature and moles of gas produce a new pressure. In the same time step, the leakage is computed and used to update the mass of the constituents including those involved in the phase changes. The combustion pressure and total pressure act on the shell to accelerate it. The acceleration is integrated with a second order accurate algorithm to calculate a new velocity. That same algorithm is used to calculate the new position of the shell in the mortar and in turn, the change in the volume, density, etc. The variables are all updated and the process is repeated for the next time interval.

Once the shell leaves the barrel, the calculation switches to the aerodynamic model. The aerodynamic force and the gravitational force decelerate the shell. These forces are integrated, again using a second order accurate algorithm, to produce a new velocity. The new velocity is used to calculate a new Reynolds number and the dependent drag coefficient. The velocity is integrated with the same second order algorithm to calculate the new shell position.

The input variables to the solver are commonly used to define a mortar set-up. These input specification variables provide a great deal of freedom in modeling various arrangements. Analyses such as the effect of shell standoff in the mortar, mortar length or the effects of shell diameter changes can be readily performed. The ambient temperature and elevation are input parameters that are used to correct for density, viscosity, pressure and temperature effects.

The atmospheric pressure model is based on a standard atmosphere so that the input parameter is elevation. With these input variables it is possible to examine the difference between a

cold day on an ocean beach versus a hot day, high in the mountains.

The wind speed input is used to calculate the drift on the shell based on the drag model and a rotation of the drag vector based on the angle of attack of the shell. The drift calculation predicts the displacement of a vertically fired shell for the given wind speed and the impact velocity and total time to impact from firing if it falls to the ground unexploded.

Since the solver calculates every detail of the firing and flight process, it can provide a detailed analysis of temperature and pressure or any other calculated parameter as a function of time, mortar position or any other independent variable. Also peak values or mean values can be calculated.

The code variables for input and output that have been selected are shown below; starting with the input parameters:

- Units (Imperial or metric; output values are given in the same units as specified for the input parameters)
- Mortar inside diameter
- Mortar length
- Shell type (spherical or cylindrical). The program was written to handle both types, but only the spherical shell portion was verified with experimental data.)
- Shell diameter (also length for cylindrical shells)
- Shell mass
- Standoff in mortar (program calculates dead volume). The standoff is defined as the distance from the equator of a spherical shell to the top of the end plug. For cylindrical shells it is the distance from the bottom of the shell to the top of the end plug. The program calculates the volume of the lift charge based on a bulk density of about ½ the particle density and makes certain that there is enough volume to accommodate the charge. If not, the shell is displaced upward to allow for the lift charge. For calculating position of the shell, a convenient reference is the bottom of cylindrical shells and equator of spherical shells.
- Black Powder mass
- Black Powder grain size (e.g., 2FA, 3Fg, "0", etc.)
- Ambient temperature
- Elevation
- Wind speed
- Ignition source (percussion cap vs. electric match or fuse)

Output calculated values are:

- Dead volume (due to standoff and Black Powder volume)
- Time to end of ignition
- Time to exit muzzle
- Unburned Black Powder at muzzle exit or powder burn time
- Barrel pressure at muzzle exit
- Maximum barrel pressure (MBP)
- Shell position at MBP
- Maximum gas temperature
- Percentage of total gas generated lost as leakage through gap
- Maximum acceleration
- Muzzle velocity
- Apogee height
- Drift at apogee due to side wind
- Time to apogee
- Terminal velocity
- Drift at impact with ground
- Side velocity at impact
- Total time

Model Verification

Two sources of empirical data were obtained. One was from Shimizu[12] for mortar internal diameters ranging from 7.6 to 30.5 cm, shown in Table 3. These data are for numerous test firings. A few parameters are missing from some test cases while other parameters are presented with statistical variations. The second set of data shown in Table 4 is from Kirkland.[15] The catalog has many tables of muzzle velocity versus powder load for muzzle loading Black Powder firearms. Only two sets of data were selected for comparison because they were specifically documented as chronographic meas-

Table 3. Shimizu's Data for Shooting Spherical Shells under "Normal Conditions".

Mortar ID (cm)	7.6	9.2	9.2	12.3	15.5	15.5	18.8	21.9	24.9	30.5
Length (cm)	44.6	81	81	89.5	103	103	119	134.4	148	142
Shell Dia. (cm)	7	8.4	8.4	11.5	14.2	14.2	17.4	20.4	23.5	29
Mass Sh. (kg)	0.208	0.22	0.115	0.53	1.25	0.61	2.115	3.17	4.83	8.27
Mass BP (kg)	0.013	0.02	0.02	0.038	0.075	0.075	0.131	0.17	0.28	0.45
Muz. Vel. (m/s)		103.9	122.2	104.9	119.6	151.9	118.7		150.5	114.8
Std. Dev.					6.5	10				
Height (m)	108	149	132	191	263	208	284	353	406	340
Std. Dev.		13.1	11.8		18.2	9.1				
Rise Time (s)	3.9	4.8	3.8		6.9	5.4	6.6	8.3	8.4	8.2
Std. Dev.		0.38	0.29		0.34	0.56				
No. of Samples	2	15	15	2	15	15	2	2	3	3
	Computed Values									
Muz. Vel. (m/s)	84.6	106.8	130.7	112.4	107.5	139.5	123.5	120.3	144.2	146.7
Height (m)	161	170.5	130.2	205.9	248.4	205.8	302.9	308.5	395	426
Rise Time (s)	5.04	4.91	3.94	5.47	6.24	5.18	6.81	6.94	7.74	8.09

Notes: The Black Powder grain size used was "0".

All computed standard deviations for data in this table are computed using the difference between the computed and measured values divided by the measured value expressed in percent. The measured standard deviations are in the parameters' units.

urements provided with configuration and powder charge specifications. One set of data is for a pistol and the other is for a rifle. The set of data for the pistol was presented with a maximum variation.

The data used covers a wide range of parameters including: barrel exit times from 1.1 to 15 ms, muzzle velocities from 282 to 2227 ft/s (86 to 679 m/s), maximum barrel pressures from 13 to 570 atm and gas leakage from 0 to 45%. These data were used in an optimization study to refine: time constants, latent heat values, leakage flow coefficient, Black Powder burn rate dependence and drag coefficients. The refined parameters were then fixed and remained unchanged for all the test cases.

Figure 2 shows the results for the flight model verification. The experimentally measured muzzle velocity from the Shimizu[12] data along with the shell diameter and mass were used for input. The figure shows the comparison of the calculated results with the measured

Table 4. Raw Data from the Dixie Gun Works, Inc.[15]

Pistol Muzzle Velocity Data for .40 cal., 9-inch Barrel Ball Size = 0.395 in.					Rifle Muzzle Velocity Data for .45 cal., 44-inch Barrel		
Charge (gr)	Velocity (fps)	Variation (± fps)	Variation (%)	Comp. Vel. (fps)	Charge (gr)	Velocity (fps)	Comp. Vel. (fps)
20	816	49	6	823.3	30	1180	1222.1
30	872	86	9.9	985	40	1560	1418.1
35	1145	110	9.6	1049.6	50	1700	1589.1
40	1178	50	4.2	1104.6	60	1800	1741
					70	1940	1877.5
Note: All tests were performed with 3Fg Black Powder. Standard Deviation = 0.0641 for the computed results.					90	2100	2117.4
					100	2140	2223.7

results. The agreement has a standard deviation, weighted by the number of test firings for each case, of 6.9%. The experimental data from Shimizu[12] show standard deviations ranging from 4.4 to 8.8%. Those data with muzzle velocity measurements had shell sizes ranging from 9.2 to 30.5 cm (3.6 to 12 in.). Some of the variation can be attributed to slight changes in surface roughness of the paper shells that could change the drag coefficients or alter the transition Reynolds number. Even so, the data cover a wide range of Reynolds numbers with agreement within the documented experimental error.

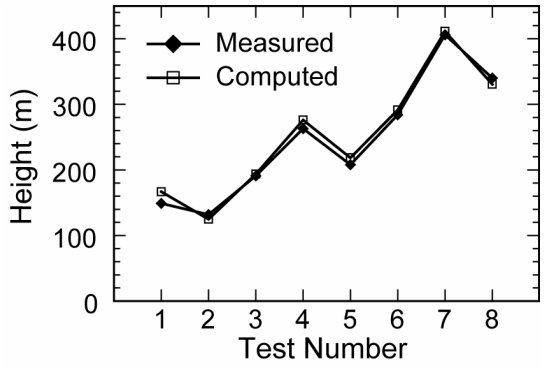

Figure 2. Drag model comparison using C_D = .4/.5 with empirical velocity as input and height as comparison.

Figure 3 shows a comparison of the computed and measured muzzle velocities using the complete firing analysis. The agreement has a weighted standard deviation of 9.5%. The experimental data only presented measurement standard deviation values for two test conditions: one value is 5.4% and the other is 6.6%. One possible reason for the slightly larger error match is the number of parameters that are sensitive to small changes. For instance, the standoff distance was not specified for the experimental data so the modeling assumption was that the distance was the amount necessary to accommodate a shell resting on a level layer of the mass of the powder specified. Another possible source of variance is the sensitivity to small changes in the diameter of the mortar or shell. Table 5 summarizes the results of a 5 mm variation in shell diameter. Almost all the velocity variations can be explained by approximately a 3% variation in shell to mortar diameter. The shell with an outside diameter of 29 cm (11.4 in.) had the greatest variation, and it can be entirely explained by a 5.2% reduction in shell diameter or increase in mortar diameter or a combination. Finally the quality of the Black Powder used can have a major effect on the results. The modeling assumed that all the Black Powder used for the experiments was of equal quality.

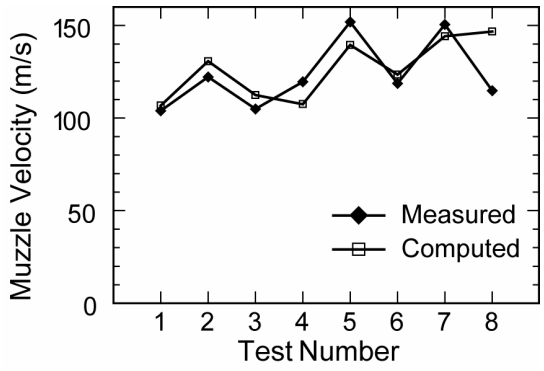

Figure 3. Comparison of computed and measured muzzle velocities.

Table 5. Analysis of Shimizu Data for Shell Diameter Variation.

Test No.[a]	2 of 8	4 of 8	8 of 8
+5 mm	160.6	127.9	161.3
0 mm	133.9	110.1	149.8
–5 mm	111.7	94.6	139
Meas. Vel. (m/s)	122.2	119.6	114.8
Shell Dia. (cm)[b]	8.4	14.2	29
Calc. Ch. (mm)[c]	–2.9	+2.7	–16.2
% Change[d]	–3.1	1.9	–5.6

Notes: The program was run with a ±5 mm variation in diameter to test the effect on muzzle velocity.

[a] The numbers represent the text number for the velocity data (8 tests).

[b] The variation in shell diameter to match velocity seems to be within experimental error (2–3%) except for the 29 cm shell that seems to be noticeably more than the others.

[c] This is the calculated change in diameter needed to match the measured velocity.

[d] This is the percent change in shell diameter.

Figure 4 shows a comparison of the computed heights. The calculations employ the complete model (both the firing and flight models). The standard deviation of the comparison, weighted by the number of measurements for each test point, is 12.1%. If the first and last points are omitted, the standard deviation drops to 7.8%. The first point was for a 7.6-cm (3-in.) mortar and did not have muzzle velocity data that would reveal sources of the disagreement. The last point was for the 30.5-cm (12-in.) mortar, where the disagreement is attributed to the difference between the computed and experimental muzzle velocities. Shimizu's data only have measurement standard deviations for 4 test conditions. For these tests, the average measurement error is 6.2%. The computed standard deviation for the same set of data is 7.8%.

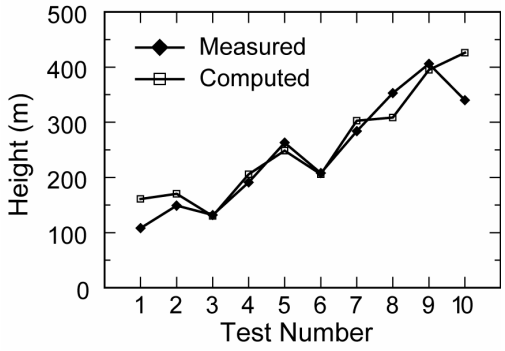

Figure 4. Computed height vs. measured height.

Figure 5 is a composite plot showing both the flight model calculations and the total model (firing and flight) calculations along with the experimental results. Except for the 30.5-cm (12-in.) result from the total (firing + flight) model, the data are in close agreement.

Figure 6 is a comparison of the rise times (time to apogee) using the full model. The comparison agreement has a standard deviation of 7.4% while the experimental data measurements have a standard deviation range from 4.9 to 10.4%. The notable result in this plot is the good agreement between computed and experimental values for the 30.5-cm (12-in.) shell. That agreement does not seem to be consistent with the previously noted agreements for muzzle velocity and height. Currently this remains a conundrum.

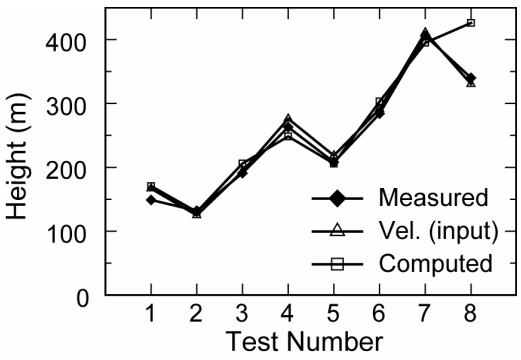

Figure 5. Height comparisons.

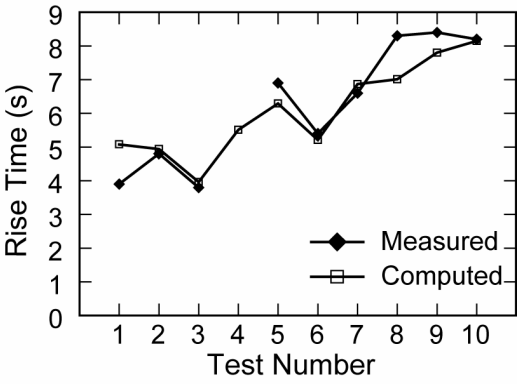

Figure 6. Shimizu rise times.

Figure 7 shows two comparisons presented on one graph. The data on the left side of the graph are for a muzzle loading, caplock Black Powder pistol, while those on the right are for a muzzle loading, flintlock Black Powder rifle. The bores are .40 and .45 caliber, respectively, and the barrel lengths are 9 and 44 in. (22.9 and 111.8 cm), respectively. Black Powder charges ranged from 20 to 40 gr (1.30 to 2.59 g) for the pistol and from 30 to 100 gr (1.94 to 6.48 g) for the rifle. The standard deviation of the comparison for the combination of pistol and rifle data is 6.4% while the experimental "variation" runs from 4.2 to 9.9% for the pistol data with no measurement error specified for the rifle data. The experimental data were for patched balls, so the model assumed a tight fit of the ball to the bore. The pistol model assumed no leakage, although the cap nipple hole would allow for some leakage, representing only 0.5% of the bore area. Countering this, the cap itself provides some sealing and the igniter charge adds to the combustion gases offsetting the leakage.

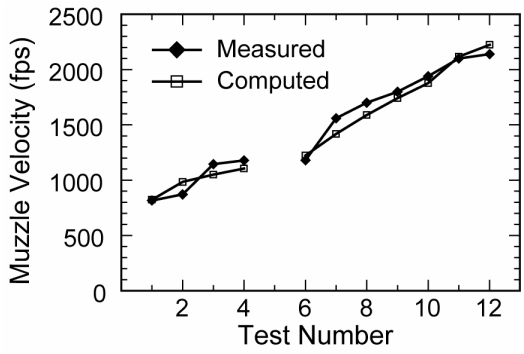

Figure 7. Dixie Gunworks data.

With all these factors, the assumed model of no leakage seems to be well within the modeling error. The rifle model assumed that there was leakage. The flash hole area represents about 2% of the bore area, and there is no obstruction to the gases escaping. To account for the leakage, the ball was modeled as having a smaller diameter producing a 0.002 in. (0.05 mm) gap between the ball and the barrel. The gap area was equal to the flash hole area. The agreement with both the pistol and rifle data seems to be within the experimental error.

Conclusions

The propellant characteristics of Black Powder and the aerodynamics of firework shells are accurately represented by the described model. The Black Powder burning model, based on the first law of thermodynamics, has a delayed release of the latent heats that is an essential element of the mortar analysis. The amount of delay is a key element in the model that allows it to analyze a wide range of test cases without changing any of the parameters. The burn rate and common thermodynamic parameters used in the model are the same or close to those found by other researchers.

A model for the leakage around the shell based on compressible flow theory appears to provide good agreement with the overall experimental data. This good agreement with experimental data ranging from large firework mortar tests down to muzzle loading rifle and pistol chronograph measurements provides confidence in the model's veracity. The numerical code based on the theoretical models provides a detailed analysis of every aspect of the thermodynamic process for mortars or muzzle-loaders.

The aerodynamic model for the shells in flight is consistent with fundamental aerodynamic principles and uses the available experimental data to determine common drag parameters that are applied equally over a wide range of test conditions. Agreement with round shell experimental data is within measurement variation. The cylindrical shell models in the code have not yet been verified but Contestabile's[13,14] experimental data should provide much of the data needed to determine the leakage and drag coefficients.

The numerical code appears to be an accurate tool that could prove useful for designing new features into display fireworks. The code could be used to design precise vertical placement of bursts. Parametric studies of mortar length, shell diameter or powder load might reveal better designs. The code can provide safety analyses (e.g., model the effects of undersized shells, incomplete insertion of a shell into the mortar or maximum barrel pressure and temperature as a function of grain size). Another safety use is for shell stress analysis wherein the computed pressure and inertial forces are required. There may even be uses for muzzle-loaders, including some of the design and safety considerations just described. The code provides a myriad of possibilities.

The model illustrates that Black Powder is a good propellant for projecting shells from a mortar because the energy release is distributed over time. This factor reduces the peak pressure to average pressure ratio thereby reducing the strength of the mortar required to contain the combustion for a given exit velocity. This same time-release factor makes Black Powder a less desirable rocket motor fuel since much of the heat is released after the combustion products pass through the nozzle thereby reducing the specific impulse.

As a final note: the characteristics of the Black Powder used for the Shimizu and Dixie Gun Works experiments were assumed to be equal except for granulation. The parameters presented in the paper are for that powder. If Black Powder of a different composition or me-

chanical incorporation is used, then the parameters may need to be adjusted for that powder.

Acknowledgements

The author acknowledges Lawrence Weinman, Will Meyerriecks, Ettore Contestabile and his friend and colleague Guenter Brune for their reviews and insightful comments. He also expresses his gratitude to his wife, June, and son, Matt, for tolerating the project that turned into an obsession.

Bibliography

1) J. A. Conkling, *Chemistry of Pyrotechnics*, Marcel Dekker, New York, NY, 1985.
2) T. L. Davis, *The Chemistry of Powder and Explosives*, Angriff Press, Hollywood, CA, 1972 (reprint of 1943 edition).
3) T. Shimizu, *Fireworks, The Art, Science and Technique*, Pyrotechnica Pubs., 1981.
4) T. Shimizu, "Ballistics of Fireworks Shells", *Proc. 13th Int'l Pyrotechnics Seminar* (1988).
5) T. Shimizu, "Balistique Intérieure: La Comparaison de Canon et le Mortier du Feu D'Artifice", *Proc. 25th Int'l Pyrotechnics Seminar* (1999).
6) A. A. Shidlovskiy, *Principles of Pyrotechnics*, American Fireworks News, 1964.
7) I. von Maltitz, *Black Powder Manufacture and Techniques*, American Fireworks News, 1997.
8) R. Sassé and J. E. Rose, "Comparison of Spherical and Ellipsoidal Form Functions foe Evaluating Black Powder", *Proc 13th Int'l Pyrotechnics Seminar* (1988).
9) D. E. G. Jones, "Interior Ballistics of Fireworks Mortars", *Proc. 1st Int'l Symp. on Fireworks,* 1992.
10) E. Freeman, "Thermodynamic Properties of Military Gun Propellants", *Prog. in Astronautics and Aeronautics,* Vol. 109 (1988) pp 103–132.
11) K. L. & B. J. Kosanke, "Shimizu Aerial Shell Ballistic Predictions (Parts 1 and 2)", *Selected Pyrotechnic Publications of K. L. and B. J. Kosanke Part 2 (1990 through 1992)*, Journal of Pyrotechnics, 1995.
12) T. Shimizu, *Fireworks from a Physical Standpoint Part III*, Pyrotechnica Pubs., 1985.
13) E. Contestabile, R. A. Augsten, T. R. Craig and J. G. McIndoe, "A study of the Firing Characteristics of High Altitude Display Fireworks", *CANMET Publication,* Ottawa, 1988.
14) E. Contestabile and R. A. Austen, "Evaluation of Large Diameter Fireworks Shells and Mortars", *Proc. 15th Int'l Pyrotechnic Seminar* (1990).
15) T. E. Kirkland, *Catalog No. 149, Dixie Gun Works*, Inc. Union City, TN, USA, 2000.
16) R. C. Weast, *Handbook of Chemistry and Physics*, 56th ed., CRC Press, 1975.
17) Elephant Black Powder, www.elephantblackpowder.com/ebp.html
18) G. V. Belov, "Thermodynamic Modeling at High Pressure and Temperature", Glushko Thermocenter, IVTAN Assoc. of Russian Academy of Sciences, 1998.
19) A. H. Shapiro, *The Dynamics and Thermodynamics of Compressible Fluid Flow*, Ronald Press Co., 1953.
20) S. F. Hoerner, *Fluid-Dynamic Drag*, Published by Author, Midland Park, NJ, 1958.
21) R. Fitzpatrick, "The Physics of Baseball Pitching", *Introduction to Computational Physics*, farside.ph.utexas.edu/teaching/329/lectures/node80.html Fall 2001.